Lancet Infect Dis 2025
Published Online
January 28, 2025
https://doi.org/10.1016/S1473-3099(25)00015-5

Virological and antigenic characteristics of SARS-CoV-2 variants LF.7.2.1, NP.1, and LP.8.1

Recently, XEC and KP.3.1.1 have surpassed KP.3 to become the globally dominant lineages of SARS-CoV-2 due to the unique N-terminal domain (NTD) mutations, including Ser31del in KP.3.1.1 and Thr22Asn and Phe59Ser in XEC.[1–7] However, several sublineages of JN.1 are increasingly out-competing XEC and KP.3.1.1, exhibiting superior growth advantages; for example, LF.7.2.1, MC.10.1, NP.1, and, most importantly, LP.8.1 (figure A, B). Notably, LF.7.2.1 contains an additional Ala475Val mutation compared with LF.7, which carries the Ser31Pro, Lys182Arg, Arg190Ser, and Lys444Arg mutations on spike, and has rapidly spread from Qatar to the Middle East and Europe. MC.10.1, a KP.3.1.1 subvariant with a rare spike mutation, Ala435Ser, shows a slightly higher growth advantage than KP.3.1.1. NP.1, which has an additional Ser446Asn relative to MC.10.1 on the receptor-binding domain (RBD), exhibits enhanced growth advantage and has spread rapidly in Canada. LP.8, a subvariant of KP.1.1, carries Ser31del, Phe186Leu, Gln493Glu, and His445Arg on spike. Importantly, LP.8.1, with an additional Arg190Ser, has surged rapidly in the USA, exhibiting the highest growth advantage among circulating variants (figure B). These novel RBD and NTD mutations have given rise to fast-evolving variants, underscoring the urgent need to evaluate their virological and antigenic characteristics for future preparedness.

We first constructed the recombinant RBD subunit of KP.3, LF.7, LF.7.2.1, MC.10.1, NP.1, and LP.8.1 and assessed their binding affinity to human ACE2 (hACE2) using surface plasmon resonance (SPR; figure C). The results show that the Ala475Val mutation in LF.7.2.1 greatly reduced RBD–ACE2 binding affinity compared with LF.7. In contrast, the binding affinities of NP.1 and LP.8.1, carrying Ser446Asn and His445Arg, respectively, did not exhibit substantial changes or only a slight decrease compared with KP.3. Given that RBD–ACE2 binding affinity alone does not fully reflect the effect of mutations on other regions or the spike trimer conformation, we constructed spike-pseudotyped vesicular stomatitis virus and assayed the efficiency of soluble hACE2 to inhibit viral entry, which indicates the ACE2 binding strength and receptor engagement

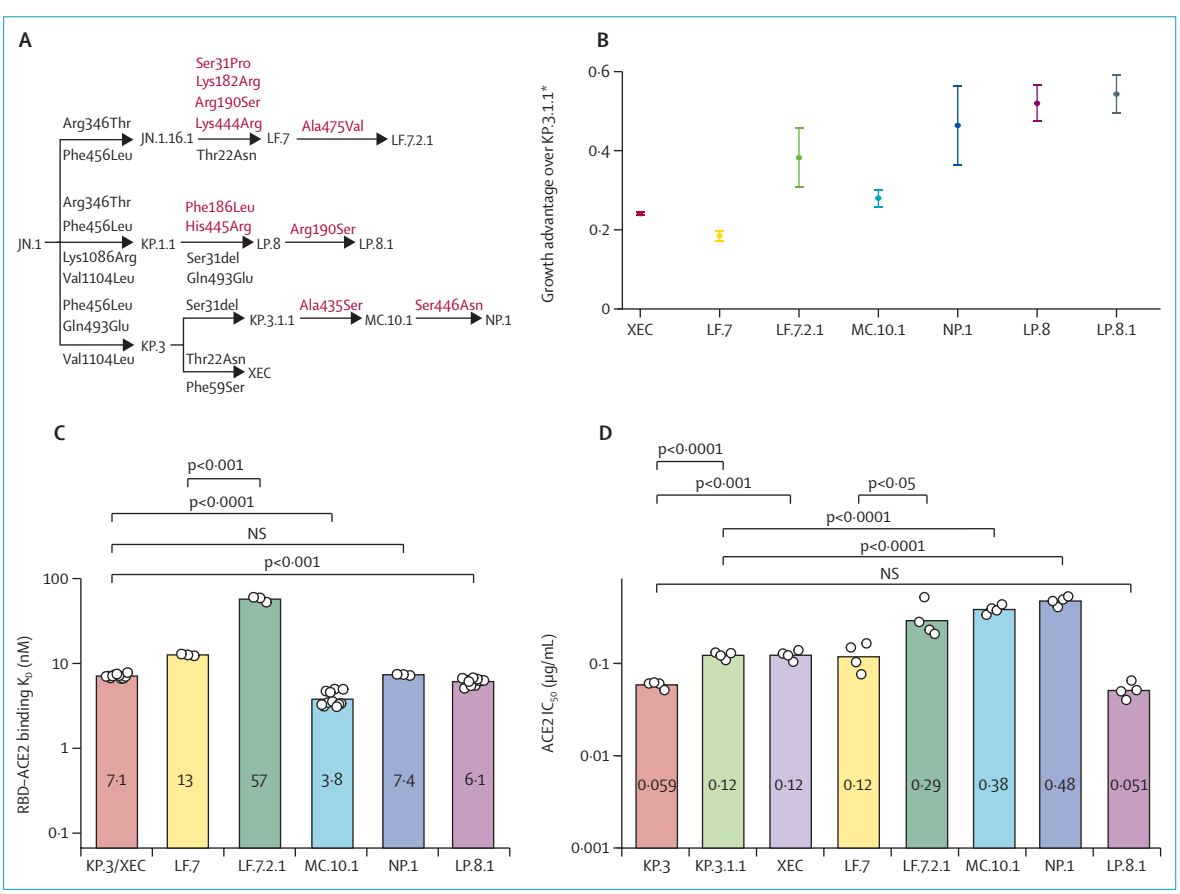

(Figure continues on next page)

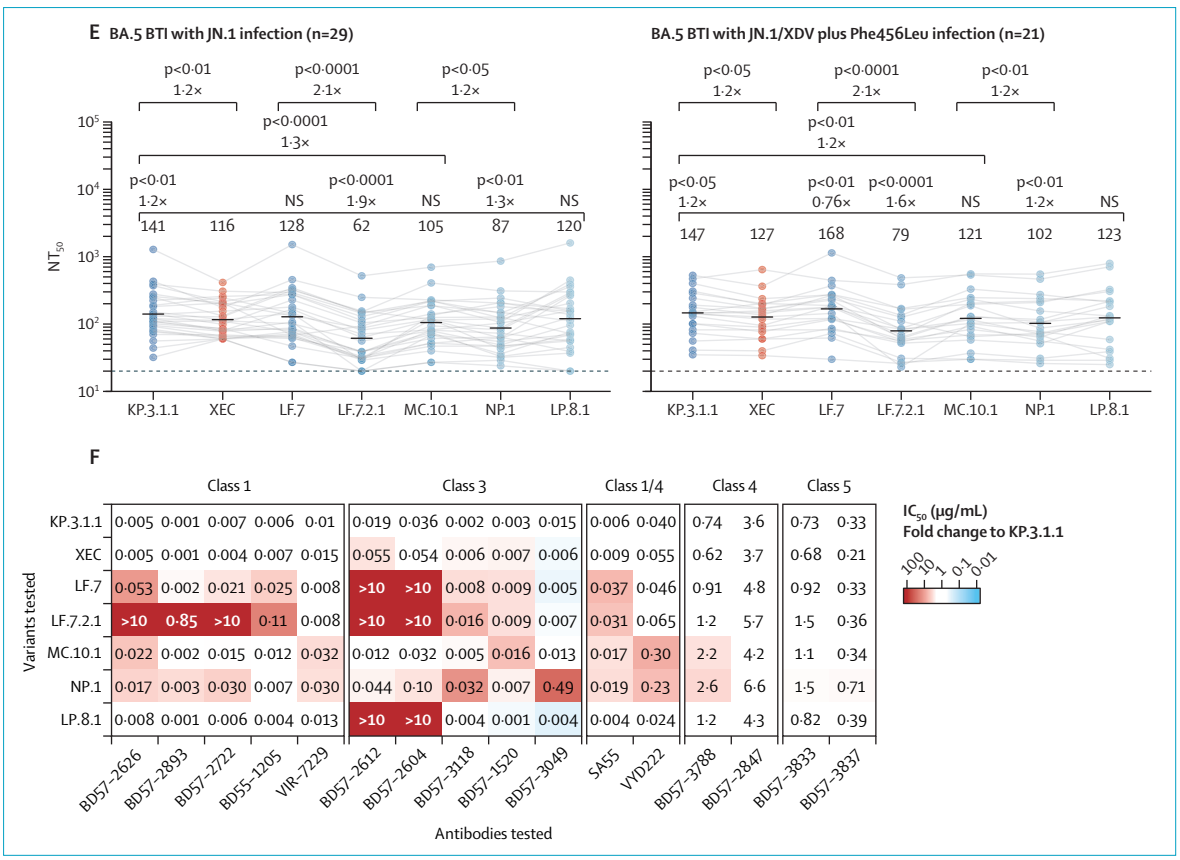

Figure: **ACE2 engagement and antibody evasion characteristics of LF.7.2.1, MC.10.1, NP.1, and LP.8.1**
(A) The evolution of the spike glycoprotein in prevalent SARS-CoV-2 variants. The mutations in red are specific to these variants, in addition to those shared with KP.3.1.1 and XEC. (B) The relative growth advantage of XEC, LF.7, LF.7.2.1, MC.10.1, NP.1, LP.8, and LP.8.1, compared with KP.3.1.1*. The relative growth advantage was calculated from daily sequence data sourced from the Global Initiative on Sharing All Influenza Data database, including sequences obtained globally from Jan 1 to Dec 9, 2024. The growth advantage was estimated with a generation time of 7 days and confidence intervals at α=0·95. The asterisk indicates all sublineages. (C) The binding affinity of KP.3/XEC, LF.7, LF.7.2.1, MC.10.1, NP.1, and LP.8.1 RBD proteins to human ACE2, established by SPR. Each circle indicates a technical replicate. Geometric mean K_D values (nM) are displayed. Log-transformed data were analysed using a two-tailed *t* test to compare the means between the two groups. (D) IC_{50} values of soluble human ACE2 against KP.3, KP.3.1.1, XEC, LF.7, LF.7.2.1, MC.10.1, NP.1, and LP.8.1 pseudoviruses. Each circle indicates a technical replicate. IC_{50} values (μg/mL) are displayed. Log-transformed data were analysed using a two-tailed *t* test to calculate p values. (E) The NT_{50} of convalescent plasma from individuals reinfected with JN.1 after BA.5 or BF.7 breakthrough infection (n=29) and those reinfected with JN.1 or XDV with Phe456Leu after BA.5 or BF.7 breakthrough infection (n=21). Plasma source cohorts and the corresponding number of samples are labelled above each panel. The dashed line indicates the limit of detection (NT_{50}=10). Geometric mean titers are labelled above each group, with fold changes and statistical significance indicated above the geometric mean titer labels. Wilcoxon rank-sum tests were used to determine p values. (F) IC_{50} values for a panel of monoclonal neutralising antibodies targeting RBD epitopes against KP.3.1.1, XEC, LF.7, LF.7.2.1, MC.10.1, NP.1, and LP.8.1 variants. The values within the table are IC_{50} values (μg/mL), while the background colour indicates the fold-change in IC_{50} relative to KP.3.1.1. The colour gradient bar represents the magnitude of IC_{50} fold-change, with red indicating IC_{50} significantly higher than, and blue indicating lower than, XEC. IC_{50}=50% inhibitory concentration. NT_{50}=50% neutralising titer. K_D=dissociation constant. SPR=surface plasmon resonance.

See Online for appendix

efficiency of the variants spike proteins (figure D). Consistent with previous findings, mutations on the NTD of KP.3.1.1 and XEC decreased the hACE2 inhibition efficiency compared with KP.3.[1-4] In concordance with the SPR results, the Ala475Val mutation in LF.7.2.1 also greatly reduced the hACE2 inhibition efficiency compared with LF.7. Surprisingly, we found that the Ala435Ser mutation significantly reduced the ACE2 binding strength in MC.10.1 and NP.1's spike compared with KP.3.1.1, but not that of the RBD, suggesting Ala435Ser might impact ACE2 engagement through altering RBD conformation. Most importantly, the mutations in LP.8.1 enhanced its spike's ACE2 binding strength to a level similar to KP.3, potentially contributing to its highest growth advantage.

Next, we evaluated the humoral immune evasion by using convalescent plasma and a panel of RBD-targeting neutralising monoclonal antibodies in pseudovirus neutralisation assays (figure E, F; appendix p 9). The plasma used in this study was obtained from two cohorts of individuals who received two or three doses of inactivated SARS-CoV-2 vaccines and subsequently experienced BA.5 or BF.7 breakthrough infections, with one cohort reinfected by JN.1 (n=29) and the other by JN.1 or XDV with Phe456Leu (n=21; appendix p 8), as previously described.[1] Compared with XEC, LF.7 showed similar or slightly reduced plasma immune

evasion, whereas LF.7.2.1 significantly increased it, making it currently the most immune evasive variant. This enhancement is attributed to the Ala475Val mutation, which significantly strengthened resistance to class 1 antibodies, consistent with previous studies (figure F; appendix p 9).[8–10] MC.10.1 exhibited higher immune evasion than KP.3.1.1, with the RBD mutation Ala435Ser reducing the neutralisation potency of class 1 and class 1/4 antibodies. Since site 435 is not located on the epitope of class 1 antibodies, this also suggests that Ala435Ser might enhance immune evasion by modulating RBD conformation, a mechanism similar to that of the NTD mutations in KP.3.1.1 and XEC. Additionally, NP.1, which carries an additional Ser446Asn when compared with MC.10.1, further enhanced immune evasion by improving its ability to escape class 3 antibodies. Importantly, LP.8.1 maintained a high level of humoral immune evasion similar to XEC, while additionally escaping recognition by certain class 3 antibodies.

In summary, LF.7.2.1 is the most immune-evasive variant, but its weak ACE2 binding affinity explains why it does not exhibit the highest growth advantage despite its strong immune evasion. Similarly, MC.10.1 and NP.1 show strong immune evasion, but the limited ACE2 binding strength of their spike restricts the growth advantage. Most importantly, we find that LP.8.1 exhibits exceptionally high ACE2 binding as well as high immune evasion, similar to XEC. The emergence of KP.3.1.1 and XEC involved a trade-off, with enhanced immune evasion achieved at the expense of ACE2 binding strength, thereby affecting their fitness. In contrast, LP.8.1 has found a way to preserve ACE2 binding similar to KP.3, while achieving immune evasion capabilities akin to XEC. These findings again highlight the strong trade-off between immune evasion and ACE2 binding strength in SARS-CoV-2 evolution, and underscores the importance of monitoring LP.8.1, especially after its recent convergent acquisition of the Ala475Val mutation.

YC has provisional patent applications for the BD series antibodies, WO2024131775A9 and WO2023151312A1, and is the founder of Singlomics Biopharmaceuticals. All other authors declare no competing interests. JL and YY contributed equally.

Editorial note: The Lancet Group takes a neutral position with respect to territorial claims in published maps and institutional affiliations.

*Jingyi Liu, Yuanling Yu, Sijie Yang, Fanchong Jian, Weiliang Song, Lingling Yu, Fei Shao, *Yunlong Cao*
yunlongcao@pku.edu.cn

Biomedical Pioneering Innovation Center (JL, SY, FJ, WS, YC), College of Future Technology (JL), College of Chemistry and Molecular Engineering (FJ), and School of Life Sciences (WS, YC), Peking University, Beijing, China; Changping Laboratory, Beijing, China (JL, YY, SY, FJ, LY, FS, YC); Peking-Tsinghua Center for Life Sciences, Tsinghua University, Beijing, China (SY)

1 Liu J, Yu Y, Jian F, et al. Enhanced immune evasion of SARS-CoV-2 variants KP.3.1.1 and XEC through N-terminal domain mutations. *Lancet Infect Dis* 2024; published online Nov 22. https://doi.org/10.1016/S1473-3099(24)00738-2.

2 Kaku Y, Uriu K, Okumura K, et al. Genotype to phenotype Japan (G2P-Japan) consortium. Virological characteristics of the SARS-CoV-2 KP.3.1.1 variant. *Lancet Infect Dis* 2024; **24:** e609.

3 Kaku Y, Okumura K, Kawakubo S, et al, and the Genotype to phenotype Japan (G2P-Japan) consortium. Virological characteristics of the SARS-CoV-2 XEC variant. *Lancet Infect Dis* 2024; **24:** e736.

4 Wang Q, Guo Y, Mellis IA, et al. Antibody evasiveness of SARS-CoV-2 subvariants KP.3.1.1 and XEC. *bioRxiv*. 2024; published online Nov 17 (preprint).

5 Arora P, Happle C, Kempf A, et al. Impact of JN.1 booster vaccination on neutralisation of SARS-CoV-2 variants KP.3.1.1 and XEC. *Lancet Infect Dis* 2024; **24:** e732–33.

6 Yang S, Yu Y, Xu Y, et al. Fast evolution of SARS-CoV-2 BA.2.86 to JN.1 under heavy immune pressure. *Lancet Infect Dis* 2024; **24:** e70–72.

7 Yang S, Yu Y, Jian F, et al. Antigenicity and infectivity characterisation of SARS-CoV-2 BA.2.86. *Lancet Infect Dis* 2023; **23:** e457–59.

8 Jian F, Wang J, Yisimayi A, et al. Evolving antibody response to SARS-CoV-2 antigenic shift from XBB to JN.1. *Nature* 2024; published online Nov 7. https://doi.org/10.1038/s41586-024-08315-x.

9 Cao Y, Jian F, Wang J, et al. Imprinted SARS-CoV-2 humoral immunity induces convergent Omicron RBD evolution. *Nature* 2023; **614:** 521–29.

10 Yisimayi A, Song W, Wang J, et al. Repeated omicron exposures override ancestral SARS-CoV-2 immune imprinting. *Nature* 2024; **625:** 148–56.